

Robust d -wave superconductivity from the Su-Schrieffer-Heeger-Hubbard model: possible route to high-temperature superconductivity

Hao-Xin Wang,¹ Yi-Fan Jiang,^{2,*} and Hong Yao^{1,†}

¹*Institute for Advanced Study, Tsinghua University, Beijing 100084, China*

²*School of Physical Science and Technology, ShanghaiTech University, Shanghai 201210, China*

(Dated: November 18, 2022)

Increasing numerical studies showed that the simplest Hubbard model on the square lattice with strong repulsion may not exhibit high-temperature superconductivity (SC). It is desired to look for other possible microscopic mechanism of realizing high-temperature SC. Here, we explore the interplay between the Su-Schrieffer-Heeger (SSH) electron-phonon coupling (EPC) and the Hubbard repulsion by density-matrix-renormalization-group (DMRG) simulations. Our state-of-the-art DMRG study showed convincingly that the interplay between strong Hubbard U and moderate Su-Schrieffer-Heeger EPC λ can induce robust d -wave SC. The SSH-type EPC can generate effective antiferromagnetic spin-exchange interactions between neighboring sites, which plays a crucial role in the interplay of inducing robust d -wave SC. Specifically, for $U = 8t$, we find that d -wave SC emerges when $\lambda > \lambda_c$ with a moderate critical value $\lambda_c = 0.1 \sim 0.2$. Our results might shed new light to understanding high-temperature SC in cuprates as well as pave a possible new route in looking for high-temperature SC in other quantum materials with both strong U and moderate λ .

Introduction: Since the discovery of cuprate high-temperature superconductivity (SC) nearly forty years ago, consensus about the microscopic mechanism for d -wave high-temperature SC has not been reached yet, which remains a key challenge in studies of strongly-correlated electronic systems [1–7]. So far the probably most studied model for understanding SC in cuprates is the Hubbard model and related t - J model [8, 9], which was believed by many to be the simplest possible model for producing both antiferromagnetic ordering and d -wave SC, depending on doping [1–3, 5–10] (for a recent review, see Ref. [11]). However, in the past several years, growing numerical studies [12–17] suggest that the simplest Hubbard model with strong Hubbard interactions in doping range relevant for hole-doped cuprates exhibits stripe order [18–20] or phase separation [21] but no d -wave superconductivity in the ground state, opposite to conclusions of high-temperature SC ground state obtained from earlier studies with various levels of approximations.

It is natural to ask what more is needed beyond the simplest Hubbard model with strong U in order to realize d -wave SC. Various intriguing works have attempted to address this issue. For instance, by including an appropriate next-nearest-neighbor hopping t' ($t' < 0$ for cuprates), d -wave SC was shown to emerge for electron doping but not for hole doping [22–26]; other related studies include doping the J_1 - J_2 spin liquid [27] or explicitly imposing stripe order in the Hubbard model [28]. Here, we propose to explore the interplay between the Su-Schrieffer-Heeger (SSH) electron-phonon coupling (EPC) and Hubbard repulsion for realizing d -wave SC mainly for two reasons. Firstly, increasing experimental and theoretical studies showed that in addition to electronic interactions EPC is crucial in understanding essential properties of various correlated quantum materials, including

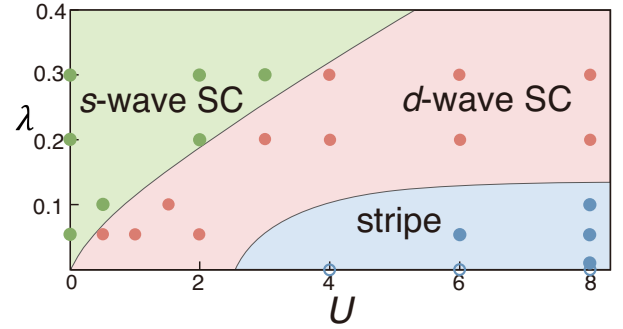


FIG. 1. The quantum phase diagram of the Su-Schrieffer-Heeger-Hubbard (SSH) model as a function of SSH electron-phonon coupling λ and Hubbard U , obtained from our state-of-the-art DMRG studies. Here, the phonon frequency $\omega_D = 5$ and hole doping concentration $\delta = 1/8$. Robust d -wave superconductivity (SC) is obtained by the interplay between strong U and moderate λ . The solid circles in this figure are DMRG results obtained in the present paper, while the open circles represent results without electron-phonon coupling ($\lambda = 0$) obtained in previous works.

high-temperature SC in cuprates [29–55] and in Fe-based SC [56–70]. It is the cooperative effect of EPC and electronic interaction that is deemed to be essential. For instance, soon after the discovery of cuprates it was proposed by Kivelson, Rokhsar, and Sethna that such interplay may induce resonating-valence-bond states [71] and recently it was shown that the interplay between Holstein EPC and strong Hubbard U may drive exotic quantum states such as pair-density-wave SC [72, 73]. Secondly, Ref. [74] made a numerical discovery that SSH-type EPC on square lattice at half-filling can induce AFM, which usually favors unconventional SC upon doping.

In this paper, we convincingly show that robust d -wave SC can be induced by doping the Su-Schrieffer-Heeger-

Hubbard (SSHH) model where the interplay between the Su-Schrieffer-Heeger EPC and the Hubbard interaction is a key for the emergence of d -wave SC. Specifically, we study the interplay between Su-Schrieffer-Heeger (SSH) EPC and the Hubbard interaction in the SSHH model on the square lattice at finite doping by large-scale density-matrix-renormalization-group (DMRG) calculations [75–77]. From state-of-the-art DMRG simulations, we obtained the quantum phase diagram by varying the dimensionless EPC constant λ and the Hubbard interaction U , as shown in Fig. 1. Three distinct phases are demonstrated in the quantum phase diagram: s -wave SC, d -wave SC, and stripe charge-density-wave (CDW) ordering. There is a large region of d -wave SC in the phase diagram, indicating the robustness of d -wave SC induced by the interplay between SSH and Hubbard interaction. For the d -wave SC obtained in the SSHH model, the Luttinger parameter $K_{sc} \approx 0.94$, which implies a divergent SC susceptibility $\chi_{sc} \sim T^{K_{sc}-2}$ as the temperature approaches zero. In particular, when $U = 8t$, the ground state exhibits stripe order for $\lambda < \lambda_c$ but d -wave SC for $\lambda > \lambda_c$ with $\lambda_c = 0.1 \sim 0.2$, which might shed new light to understanding high-temperature SC in cuprates.

Model: We consider the SSHH model on the square lattice with the following Hamiltonian

$$H = -t \sum_{\langle ij \rangle} (c_{i\sigma}^\dagger c_{j\sigma} + h.c.) + U \sum_i n_{i\uparrow} n_{i\downarrow} + \sum_{\langle ij \rangle} \left(\frac{P_{ij}^2}{2M} + \frac{K}{2} X_{ij}^2 \right) + \alpha \sum_{\langle ij \rangle} X_{ij} (c_{i\sigma}^\dagger c_{j\sigma} + h.c.), \quad (1)$$

where $\langle ij \rangle$ denotes nearest-neighbor (NN) bond, $c_{i\sigma}^\dagger$ creates an electron on site i with polarization $\sigma = \uparrow/\downarrow$, $n_{i\sigma} = c_{i\sigma}^\dagger c_{i\sigma}$, X_{ij} and P_{ij} are the displacement and momentum operators of the optical SSH phonon on the NN bond $\langle ij \rangle$. The SSH phonon frequency $\omega_D = \sqrt{K/M}$ and the strength of EPC is defined as $\lambda = \alpha^2/(KW)$, where $W = 8t$ is the typical band width of the square lattice. In the following, we set $t = 1$ as the energy unit and focus on repulsive Hubbard interaction $U > 0$ with hole doping concentration $\delta = 1/8$ and phonon frequency $\omega_D = 5$. We believe the results obtained in the present work apply more generally.

To gain some insights, we first discuss the SSHH model in the anti-adiabatic (AA) limit ($\omega_D \rightarrow \infty$ or $M \rightarrow 0$), which was proposed in Ref. [74] for understanding AFM ordering at half filling even without U . In the AA limit, the SSHH model can be reduced to the following effective model by integrating out phonons [74]

$$H_{AA} = -t \sum_{\langle ij \rangle} (c_{i\sigma}^\dagger c_{j\sigma} + H.c.) + U \sum_i n_{i\uparrow} n_{i\downarrow} + J \sum_{\langle ij \rangle} [\mathbf{S}_i \cdot \mathbf{S}_j - \frac{1}{2} (\Delta_i^\dagger \Delta_j + h.c.) + \frac{1}{4} n_i n_j], \quad (2)$$

where $J = 2\alpha^2/K$ is the strength of interactions mediated by optical phonons in the AA limit when U is not considered, \mathbf{S}_i is the spin-1/2 operator, $\Delta_i^\dagger = c_{i\uparrow}^\dagger c_{i\downarrow}^\dagger$ is the on-site pair creation operator, and $n_i = n_{i\uparrow} + n_{i\downarrow}$ is the density operator. For finite doping, it is clear that the pair hopping term $-J/2(\Delta_i^\dagger \Delta_j + h.c.)$ favors onsite s -wave pairing. However, such onsite s -wave pairing will be strongly suppressed by the Hubbard repulsion U . Fortunately, the spin exchange coupling $J\mathbf{S}_i \cdot \mathbf{S}_j$ can favor d -wave pairing on bonds which cannot be suppressed by the onsite Hubbard repulsion U , yielding the possibility of a d -wave SC when the s -wave components are sufficiently suppressed by the onsite repulsive U [74, 78].

For the general SSHH model with finite ω_D and finite U , we employ DMRG to study ground state properties of the model on $L_x \times L_y$ cylinder with open boundary condition (OBC) along x -direction but periodic boundary condition (PBC) along y -direction, where L_x and L_y denote the linear size along x and y directions, respectively. SC properties of the model are diagnosed by computing equal-time pair-pair correlations in the ground state:

$$\Phi_{\alpha\beta}(r) = \frac{1}{L_y} \sum_{y=1}^{L_y} \langle \Delta_\alpha^\dagger(x_0, y) \Delta_\beta(x_0 + r, y) \rangle, \quad (3)$$

where $\Delta_\alpha^\dagger(x, y) = \frac{1}{\sqrt{2}} [c_{(x,y),\uparrow}^\dagger c_{(x,y)+\alpha,\downarrow}^\dagger - c_{(x,y),\downarrow}^\dagger c_{(x,y)+\alpha,\uparrow}^\dagger]$ is the spin-singlet pair creation operator on site ($\alpha = 0$) or on NN bond ($\alpha = \hat{x}, \hat{y}$) and x_0 is the reference point. To minimize the boundary effect of the finite system, for various L_x , we calculate the $\Phi_{\alpha\beta}(r = \frac{L_x}{2} - 1)$ with x_0 around $L_x/4$. Density-density and spin-spin correlation functions are computed similarly. In our calculations, we keep the bond dimensions up to $D = 18000$ to obtain reliable results with typical truncation error $\varepsilon \sim 2 \times 10^{-6}$. All the data shown in the plots have been extrapolated to the $\varepsilon \rightarrow 0$ limit using quadratic fitting. Numerical details are discussed in the Supplemental Materials [79].

The main results of this work are illustrated in the quantum phase diagram of SSHH model as a function of Hubbard U and the dimensionless SSH EPC constant λ , as shown in Fig. 1. We identify three phases according to their long-range charge and pairing properties: (a) an on-site s -wave SC phase characterized by dominant quasi-long-range SC correlation and subdominant quasi-long-range charge density correlation; (b) The d -wave SC phase characterized by dominant SC correlation with d -wave symmetry and subdominant charge-density correlation; (c) stripe CDW phase with short-range SC correlation and long-range CDW ordering.

The s -wave SC for finite λ and zero U : When $U = 0$, there is only SSH electron-phonon interaction, and the SSHH model is reduced to the SSH phonon model. At half filling, the ground state of the SSH phonon model is either AFM or valence bond solid (VBS) depending on the value of λ [74]. It is expected that doping holes into the SSH phonon model can induce super-

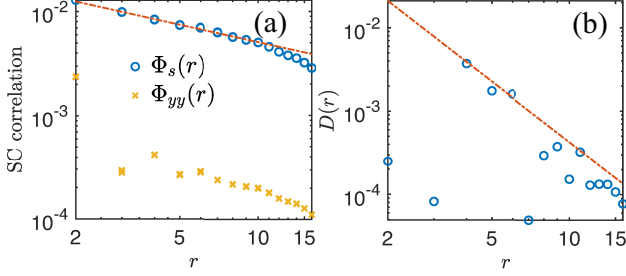


FIG. 2. Properties of the s -wave SC phase for the SSHH model with $\lambda = 0.3$ and $U = 0$ on $L_x = 48$ cylinder. (a) Onsite pair-pair and bond pair-pair correlation are plotted, respectively. (b) Density-density correlation is plotted.

conductivity. We first performed our DMRG calculations of the SSH phonon model (namely $U = 0$) at finite doping ($\delta = 1/8$) for various values of EPC coupling λ .

Our DMRG calculations of the model with $U = 0$ and various λ showed that the onsite s -wave pairing is always the most dominant pairing channel, as shown in Fig. 1. Besides the dominant onsite s -wave pairing Φ_s , there is also subdominant bond d -wave pairing Φ_{yy} , as shown in Fig. 2(a), which can be understood heuristically from the AA limit. In the AA limit, the effective pairing hopping term $-J/2(\Delta_i^\dagger \Delta_j + h.c.)$ which favors onsite s -wave pairing is more effective in inducing SC than the effective AF spin-exchange interaction $J\mathbf{S}_i \cdot \mathbf{S}_j$ which tends to favor bond d -wave pairing. For $\lambda = 0.3$ and $U = 0$, we find that the leading SC correlation function is the quasi-long-range on-site correlation $\Phi_s(r) \propto r^{-K_{sc}}$ with Luttinger exponent $K_{sc} = 0.56 \pm 0.04$, while the on-bond $\Phi_{yy}(r)$ is roughly two orders of magnitude weaker than $\Phi_s(r)$, as shown in Fig. 2. We also measured the density-density correlation function which is also quasi-long-range, $D(r) \propto r^{-K_c}$, with a much larger exponent $K_c = 2.4 \pm 0.2$, as shown in Fig. 2(b). The spin and single-particle excitations are gapped in the s -wave SC phase (see the SM [79] for details).

The d -wave SC for moderate EPC and large U : When fixing λ , i.e. $\lambda = 0.3$, and gradually increasing U from zero, the onsite Hubbard repulsion naturally suppresses the onsite s -wave pairing tendency but leaves the bond d -wave pairing channel nearly unaffected. Consequently, we expect that with increasing U the onsite s -wave pairing should become increasingly weaker such that the system could be driven into a d -wave SC phase by sufficiently large U . Note that it was shown that d -wave SC with exponentially-small T_c can appear for weak U and zero λ from perturbative RG analysis [80] as well as for weak U and weak λ [81]. In this paper we focus more on strong U which is the case of cuprates and explore how robust d -wave SC can emerge from the interplay between strong U and moderate λ .

In our DMRG calculation, the competition between d -

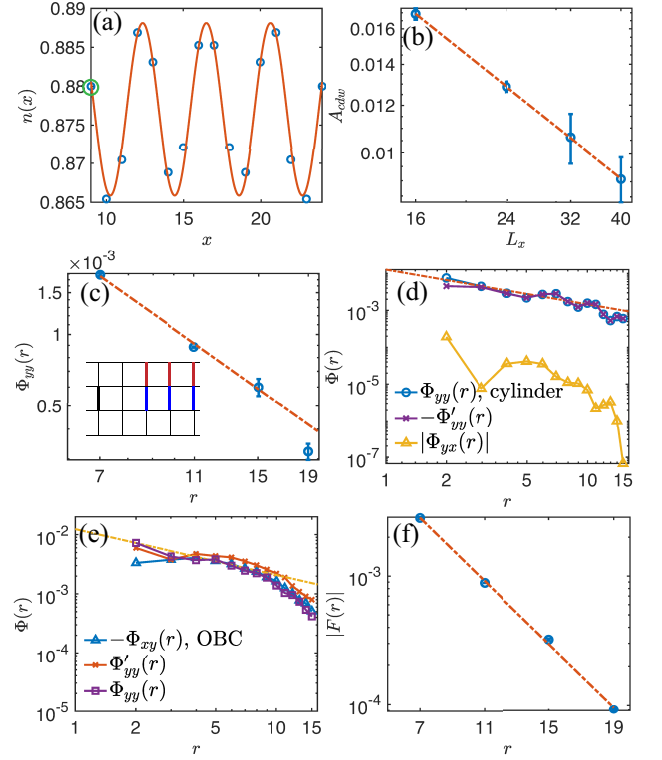


FIG. 3. Properties of the d -wave SC phase for the SSHH model with $\lambda = 0.3$ and $U = 8$, which is deep inside the d -wave SC phase. (a) The charge density profile $n(x)$ on the $L_x = 32$ cylinder fitted by the function $n(x) = A_{cdw} \cos(Qx + \theta) + n_0$ (red line). The point marked by the green circle is the reference point x_0 in the correlation function. (b) Finite size scaling of the CDW amplitude $A_{cdw}(L_x)$ obtained on the cylinders with length $L_x = 16 \sim 40$. The errorbars come from confidence intervals of the finite bond dimension extrapolations. (c) The pair-pair correlation $\Phi_{yy}(r)$ on the y -bond as a function of distance $r = L_x/2 - 1$ in a double-logarithmic plot. (d) The pair-pair correlation functions between different types of bonds Φ'_{yy} , Φ''_{yy} and Φ_{yx} on $L_x = 32$ cylinders. Red line shows the fitting of $\Phi_{yy}(r)$ with $K_{sc} = 0.94 \pm 0.2$. (e) The same correlation functions as in (d) but for strip geometry where the fitted $K_{sc} = 0.77 \pm 0.2$. (f) The spin-spin correlation $F(r)$ in a semi-logarithmic plot.

wave and s -wave SC is studied by comparing the on-site s -wave pair-pair correlation function $\Phi_s(r)$ and the bond pair-pair correlation $\Phi_{yy}(r)$. For $\lambda = 0.3$ and $U = 0$, the on-site s -wave pair-pair correlation $\Phi_s(r)$ is roughly two orders of magnitude stronger than the bond pair-pair correlation $\Phi_{yy}(r)$. When U is increased from zero, the amplitude of $\Phi_s(r)$ is quickly suppressed and eventually becomes a sub-dominant correlation than bond d -wave pairing when $U \gtrsim 3$, as shown in Fig. 1 and in SM [79].

We choose $\lambda = 0.3$ and $U = 8$, which is deep inside the d -wave SC phase, as a representative model to investigate the properties of this d -wave SC phase and its possible relevance to cuprates. For dominant bond pair-pair correlations, aside from the extended s -wave and usual

d -wave pairing the special geometry of the 4-leg cylinder also allows the appearance of “plaquette” d -wave pairing, as pointed out in Ref. [82, 83]. To distinguish between these three candidate pairing symmetries, we further measure the pair-pair correlation functions $\Phi'_{yy}(r)$ on cylinder and on strip geometry with open boundary conditions along both directions, respectively. Here Φ'_{yy} is pair-pair correlations on two bonds which are separated by distance r along the x direction and distance one along y direction. In the inset of Fig. 3(c), we show the correlation coordinates of $\Phi'_{yy}(r)$ as the black and red bonds. In Fig. 3(d) and Fig. 3(e), we plot Φ_{yy} , Φ'_{yy} , and Φ_{yx} measured on the $L_x = 32$ cylinder and strip, respectively. On both systems, we observe the quasi-long-range SC correlation at long distance with exponent $K_{sc} \approx 0.94$ for cylinder and $K_{sc} \approx 0.77$ for strip, respectively. However, their pair symmetries are different. On the 4-leg cylinder, the fact that $\Phi_{yy}(r) \simeq -\Phi'_{yy}(r) \gg |\Phi_{yx}(r)| > 0$ implies that the system forms a plaquette d -wave SC state which shares similar properties with the one reported in the pure Hubbard model with negative next-nearest-neighbor t' term. While on the 4-leg strip, it is clearly ordinary d -wave pairing with $\Phi_{yy}(r) \simeq \Phi'_{yy}(r) \simeq -\Phi_{yx}(r)$, which implies that the d -wave pairing induced by the interplay between EPC and Hubbard interaction is the usual d -wave on wider and 2D systems where the 4-site special plaquette relevant only to 4-leg ladders no longer exists.

We further study the charge-density properties of the representative model with $U = 8$ and $\lambda = 0.3$ by measuring the density profile $n(x) = \frac{1}{L_y} \sum_{y=1}^{L_y} \langle n(x, y) \rangle$ in the bulk of the systems. As shown in Fig. 3(a), the density profile exhibits a clear “half-filled” stripe with wave-length 4 for doping $\delta = 1/8$, i.e., half a doped hole in each CDW unit cell. The low energy physics in the charge sector can be determined by the long distant behavior of density-density correlation. For the ground state with gapless charge excitations, the spatial decay of the correlation is dominated by a power-law function with charge exponent K_c . On the finite system, the Luttinger parameter K_c can be extracted from $A_{cdw}(L_x) \propto L_x^{-K_c/2}$, where $A_{cdw}(L_x)$ is the CDW amplitude in the middle of the cylinders with length L_x . As illustrated in Fig. 3(b), the A_{cdw} obtained on a series of cylinders with $L_x = 16 \sim 40$ show a clear power-law decaying with exponent $K_c = 1.35 \pm 0.01$, indicating the charge gap vanishes in the d -wave phase. We also observe consistent results from the Friedel oscillation induced by the open boundary of the cylinder (details are provided in the SM [79]). We further investigated the magnetic properties of the ground state by measuring the spin-spin correlation functions defined as $F(r) = \frac{1}{L_y} \sum_{y=1}^{L_y} \vec{S}_{x_0, y} \cdot \vec{S}_{x_0+r, y}$, where $\vec{S}_{x, y}$ is the spin operator on site (x, y) . Following the same procedure used for SC correlation, we find a short-range spin-spin correlation $F(r) \propto \exp(-r/\xi_s)$ with correlation length

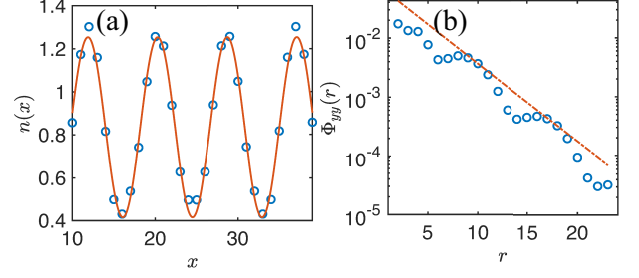


FIG. 4. Properties of the stripe phase for strong U and small λ . (a) Charge density profile of $\lambda = 0.1$ and $U = 8$ model on $L_x = 48$ cylinder. The dominant CDW order with wavelength 8 is formed at $\delta = 1/8$ doping. (b) SC pair-pair correlation function in the semi-logarithmic plot for the same system.

$\xi_s = 3.54$ as shown in Fig. 3(f), indicating a finite spin gap of the d -wave SC phase at $U = 8$ and $\lambda = 0.3$.

The stripe phase for strong U and $\lambda < \lambda_c$: There were plenty pieces of evidence that the ground state of the pure Hubbard model (namely $\lambda = 0$) with doping $\delta = 1/8$ and moderate U ($U = 4 \sim 8$) exhibits a long-range filled-stripe CDW order [12, 13, 16, 84]. Our DMRG study also found this filled-stripe state characterized by the long-range CDW order with ordering momentum $Q_{CDW} = 2\pi/8$ and short-range SC correlation on four-leg cylinders for moderate U . We then study the fate of this filled-stripe state by increasing EPC λ while fixing U . For instance, when $U = 8$ we find that the filled-stripe phase is stable against small λ , e.g., the SC correlation function $\Phi_{yy}(r) \propto e^{-r/\xi_{sc}}$ still decays exponentially with a long correlation length $\xi_{sc} = 3.3$ for $\lambda = 0.1$, as shown in Fig. 4. When EPC is further increased to $\lambda \geq 0.2$, the system is driven into the d -wave SC phase by the SSH phonon. Consequently, for $U = 8$ and $\lambda > \lambda_c$ with $\lambda_c = 0.1 \sim 0.2$, robust d -wave SC emerges. This strong coupling d -wave SC phase is the key result of this paper, which implies that the interplay between Hubbard repulsion and SSH electron-phonon coupling plays a crucial role in inducing d -wave superconductivity.

Discussion and concluding remarks: In conclusion, from the state-of-the-art DMRG calculations, we have shown convincing evidence that the interplay between moderate SSH-type EPC and strong Hubbard U on the square lattice can induce robust d -wave SC, which cannot be obtained from either moderate EPC or strong Hubbard repulsion alone. The onsite s -wave SC is induced when there is only EPC, while the stripe CDW order is obtained for strong Hubbard interaction without EPC. We also established the dominant SC correlations and subdominant CDW correlations by finite-size scaling in the d -wave SC phase, with $K_{sc} \approx 0.94$ and divergent SC susceptibility. Although the error bar in numerical values of the Luttinger exponents obtained from DMRG is not that small, they are already close to the physical properties of a Luther-Emery liquid, and the d -wave SC

state we obtained exhibits most of the qualitative properties of a Luther-Emery liquid. To determine those exponents more accurately, it is desired to study the model on ladders with much larger L_x and keep more states in DMRG, which can be explored in the future.

The d -wave SC states obtained for strong U and moderate λ could have potential relevance for understanding the d -wave SC in cuprates which have both strong onsite Coulomb repulsion and moderate EPC. For $U = 8$, our DMRG calculations showed that d -wave SC phase emerges for $\lambda > \lambda_c$ with $\lambda_c = 0.1 \sim 0.2$. For cuprates, recent experiments estimate that its EPC is about $\lambda = 0.2 \sim 0.3$ [54, 85]. Moreover, we think that our findings presented in this paper might pave a new route in looking for unconventional superconductivity and even high-temperature superconductivity in quantum materials with corroborate electron-phonon and electron-electron interactions.

Acknowledgement: We would like to thank Hong-Chen Jiang, Steve Kivelson, Rong-Yang Sun, Yi-Ming Wu, and Zheng-Zhi Wu for helpful discussions, and are especially grateful to Xun Cai and Zi-Xiang Li for earlier collaboration on this topic. This work is supported in part by the NSFC under Grant No. 11825404 (HXW and HY), the MOSTC Grants No. 2018YFA0305604 and No. 2021YFA1400100 (HY), and Shanghai Pujiang Program under Grant No.21PJ1410300 (YFJ).

* jiangyf2@shanghaitech.edu.cn

† yaohong@tsinghua.edu.cn

- [1] B. Keimer, S. A. Kivelson, M. R. Norman, S. Uchida, and J. Zaanen, *Nature* **518**, 179 (2015).
- [2] J. C. S. Davis and D.-H. Lee, *Proceedings of the National Academy of Sciences* **110**, 17623 (2013).
- [3] E. Dagotto, *Rev. Mod. Phys.* **66**, 763 (1994).
- [4] A. Damascelli, Z. Hussain, and Z.-X. Shen, *Rev. Mod. Phys.* **75**, 473 (2003).
- [5] P. A. Lee, N. Nagaosa, and X.-G. Wen, *Rev. Mod. Phys.* **78**, 17 (2006).
- [6] D. J. Scalapino, *Rev. Mod. Phys.* **84**, 1383 (2012).
- [7] E. Fradkin, S. A. Kivelson, and J. M. Tranquada, *Rev. Mod. Phys.* **87**, 457 (2015).
- [8] P. W. Anderson, *Science* **235**, 1196 (1987).
- [9] F. C. Zhang and T. M. Rice, *Phys. Rev. B* **37**, 3759 (1988).
- [10] P. W. Anderson, P. A. Lee, M. Randeria, T. M. Rice, N. Trivedi, and F. C. Zhang, *Journal of Physics: Condensed Matter* **16**, R755 (2004).
- [11] D. P. Arovas, E. Berg, S. A. Kivelson, and S. Raghu, *Annual Review of Condensed Matter Physics* **13**, 239 (2022).
- [12] J. P. F. LeBlanc, A. E. Antipov, F. Becca, I. W. Bulik, G. K.-L. Chan, C.-M. Chung, Y. Deng, M. Ferrero, T. M. Henderson, C. A. Jiménez-Hoyos, E. Kozik, X.-W. Liu, A. J. Millis, N. V. Prokof'ev, M. Qin, G. E. Scuseria, H. Shi, B. V. Svistunov, L. F. Tocchio, I. S. Tupitsyn, S. R. White, S. Zhang, B.-X. Zheng, Z. Zhu, and E. Gull (Simons Collaboration on the Many-Electron Problem), *Phys. Rev. X* **5**, 041041 (2015).
- [13] B.-X. Zheng, C.-M. Chung, P. Corboz, G. Ehlers, M.-P. Qin, R. M. Noack, H. Shi, S. R. White, S. Zhang, and G. K.-L. Chan, *Science* **358**, 1155 (2017).
- [14] E. W. Huang, C. B. Mendl, S. Liu, S. Johnston, H.-C. Jiang, B. Moritz, and T. P. Devereaux, *Science* **358**, 1161 (2017).
- [15] E. W. Huang, C. B. Mendl, H.-C. Jiang, B. Moritz, and T. P. Devereaux, *npj Quantum Materials* **3**, 22 (2018).
- [16] M. Qin, C.-M. Chung, H. Shi, E. Vitali, C. Hubig, U. Schollwöck, S. R. White, and S. Zhang (Simons Collaboration on the Many-Electron Problem), *Phys. Rev. X* **10**, 031016 (2020).
- [17] S. Sorella, *arXiv:2101.07045* (2021).
- [18] J. Zaanen and O. Gunnarsson, *Phys. Rev. B* **40**, 7391 (1989).
- [19] H. J. Schulz, *J. Phys. France* **50**, 2833 (1989).
- [20] S. A. Kivelson, I. P. Bindloss, E. Fradkin, V. Oganesyan, J. M. Tranquada, A. Kapitulnik, and C. Howald, *Rev. Mod. Phys.* **75**, 1201 (2003).
- [21] V. J. Emery, S. A. Kivelson, and H. Q. Lin, *Phys. Rev. Lett.* **64**, 475 (1990).
- [22] H.-C. Jiang and T. P. Devereaux, *Science* **365**, 1424 (2019).
- [23] Y.-F. Jiang, J. Zaanen, T. P. Devereaux, and H.-C. Jiang, *Phys. Rev. Research* **2**, 033073 (2020).
- [24] S. Gong, W. Zhu, and D. N. Sheng, *Phys. Rev. Lett.* **127**, 097003 (2021).
- [25] S. Jiang, D. J. Scalapino, and S. R. White, *Proceedings of the National Academy of Sciences* **118**, e2109978118 (2021).
- [26] C. Peng, Y. Wang, J. Wen, Y. Lee, T. Devereaux, and H.-C. Jiang, *arxiv:2206.03486*.
- [27] H.-C. Jiang and S. A. Kivelson, *Phys. Rev. Lett.* **127**, 097002 (2021).
- [28] H.-C. Jiang and S. A. Kivelson, *Proceedings of the National Academy of Sciences* **119**, e2109406119 (2022).
- [29] A. Lanzara, P. V. Bogdanov, X. J. Zhou, S. A. Kellar, D. L. Feng, E. D. Lu, T. Yoshida, H. Eisaki, A. Fujimori, K. Kishio, J.-I. Shimoyama, T. Noda, S. Uchida, Z. Hussain, and Z.-X. Shen, *Nature* **412**, 510 (2001).
- [30] Z.-X. Shen, A. Lanzara, S. Ishihara, and N. Nagaosa, *Philosophical Magazine B* **82**, 1349 (2002).
- [31] T. Cuk, F. Baumberger, D. H. Lu, N. Ingle, X. J. Zhou, H. Eisaki, N. Kaneko, Z. Hussain, T. P. Devereaux, N. Nagaosa, and Z.-X. Shen, *Phys. Rev. Lett.* **93**, 117003 (2004).
- [32] A. S. Mishchenko and N. Nagaosa, *Phys. Rev. Lett.* **93**, 036402 (2004).
- [33] X. J. Zhou, J. Shi, T. Yoshida, T. Cuk, W. L. Yang, V. Brouet, J. Nakamura, N. Mannella, S. Komiya, Y. Ando, F. Zhou, W. X. Ti, J. W. Xiong, Z. X. Zhao, T. Sasagawa, T. Kakeshita, H. Eisaki, S. Uchida, A. Fujimori, Z. Zhang, E. W. Plummer, R. B. Laughlin, Z. Hussain, and Z.-X. Shen, *Phys. Rev. Lett.* **95**, 117001 (2005).
- [34] O. Rösch, O. Gunnarsson, X. J. Zhou, T. Yoshida, T. Sasagawa, A. Fujimori, Z. Hussain, Z.-X. Shen, and S. Uchida, *Phys. Rev. Lett.* **95**, 227002 (2005).
- [35] J. Lee, K. Fujita, K. McElroy, J. A. Slezak, M. Wang, Y. Aiura, H. Bando, M. Ishikado, T. Masui, J.-X. Zhu, A. V. Balatsky, H. Eisaki, S. Uchida, and J. C. Davis, *Nature* **442**, 546 (2006).
- [36] D. Reznik, L. Pintschovius, M. Ito, S. Iikubo, M. Sato, H. Goka, M. Fujita, K. Yamada, G. D. Gu, and J. M.

- Tranquada, *Nature* **440**, 1170 (2006).
- [37] C. Honerkamp, H. C. Fu, and D.-H. Lee, *Phys. Rev. B* **75**, 014503 (2007).
- [38] C. Gadermaier, A. S. Alexandrov, V. V. Kabanov, P. Kusar, T. Mertelj, X. Yao, C. Manzoni, D. Brida, G. Cerullo, and D. Mihailovic, *Phys. Rev. Lett.* **105**, 257001 (2010).
- [39] S. Johnston, F. Vernay, B. Moritz, Z.-X. Shen, N. Nagaosa, J. Zaanen, and T. P. Devereaux, *Phys. Rev. B* **82**, 064513 (2010).
- [40] E. A. Nowadnick, S. Johnston, B. Moritz, R. T. Scalettar, and T. P. Devereaux, *Phys. Rev. Lett.* **109**, 246404 (2012).
- [41] S. Johnston, E. A. Nowadnick, Y. F. Kung, B. Moritz, R. T. Scalettar, and T. P. Devereaux, *Phys. Rev. B* **87**, 235133 (2013).
- [42] I. V. Sankar and A. Chatterjee, *The European Physical Journal B* **87**, 154 (2014).
- [43] E. A. Nowadnick, S. Johnston, B. Moritz, and T. P. Devereaux, *Phys. Rev. B* **91**, 165127 (2015).
- [44] J. Greitemann, S. Hesselmann, S. Wessel, F. F. Assaad, and M. Hohenadler, *Phys. Rev. B* **92**, 245132 (2015).
- [45] S. Nath, N. S. Mondal, and N. K. Ghosh, *Journal of Superconductivity and Novel Magnetism* **28**, 1687 (2015).
- [46] Y.-H. Liu, R. M. Konik, T. M. Rice, and F.-C. Zhang, *Nature Communications* **7**, 10378 (2016).
- [47] S. Nath and N. K. Ghosh, *Journal of Low Temperature Physics* **182**, 1 (2016).
- [48] Y. Zhong, Y. Wang, S. Han, Y.-F. Lv, W.-L. Wang, D. Zhang, H. Ding, Y.-M. Zhang, L. Wang, K. He, R. Zhong, J. A. Schneeloch, G.-D. Gu, C.-L. Song, X.-C. Ma, and Q.-K. Xue, *Science Bulletin* **61**, 1239 (2016).
- [49] N. C. Costa, T. Blommel, W.-T. Chiu, G. Batrouni, and R. T. Scalettar, *Phys. Rev. Lett.* **120**, 187003 (2018).
- [50] Y. He, M. Hashimoto, D. Song, S.-D. Chen, J. He, I. M. Vishik, B. Moritz, D.-H. Lee, N. Nagaosa, J. Zaanen, T. P. Devereaux, Y. Yoshida, H. Eisaki, D. H. Lu, and Z.-X. Shen, *Science* **362**, 62 (2018).
- [51] Y. He, S. Wu, Y. Song, W.-S. Lee, A. H. Said, A. Alatas, A. Bosak, A. Girard, S. M. Souliou, A. Ruiz, M. Heping, M. Bluschke, E. Schierle, E. Weschke, J.-S. Lee, H. Jang, H. Huang, M. Hashimoto, D.-H. Lu, D. Song, Y. Yoshida, H. Eisaki, Z.-X. Shen, R. J. Birgeneau, M. Yi, and A. Frano, *Phys. Rev. B* **98**, 035102 (2018).
- [52] N. C. Costa, K. Seki, S. Yunoki, and S. Sorella, *Communications Physics* **3**, 80 (2020).
- [53] Y. Wang, I. Esterlis, T. Shi, J. I. Cirac, and E. Demler, *Phys. Rev. Research* **2**, 043258 (2020).
- [54] Z. Chen, Y. Wang, S. N. Rebec, T. Jia, M. Hashimoto, D. Lu, B. Moritz, R. G. Moore, T. P. Devereaux, and Z.-X. Shen, *Science* **373**, 1235 (2021).
- [55] J.-Q. Fan, X.-Q. Yu, F.-J. Cheng, H. Wang, R. Wang, X. Ma, X.-P. Hu, D. Zhang, X.-C. Ma, Q.-K. Xue, and C.-L. Song, *National Science Review* **9**, nwab225 (2021).
- [56] Q.-Y. Wang, Z. Li, W.-H. Zhang, Z.-C. Zhang, J.-S. Zhang, W. Li, H. Ding, Y. Ou, P. Deng, K. Chang, J. Wen, C.-L. Song, K. He, J.-F. Jia, S.-H. Ji, Y.-Y. Wang, L.-L. Wang, X. Chen, X.-C. Ma, and Q.-K. Xue, *Chinese Physics Letters* **29**, 037402 (2012).
- [57] J. J. Lee, F. T. Schmitt, R. G. Moore, S. Johnston, Y.-T. Cui, W. Li, M. Yi, Z. K. Liu, M. Hashimoto, Y. Zhang, D. H. Lu, T. P. Devereaux, D.-H. Lee, and Z.-X. Shen, *Nature* **515**, 245 (2014).
- [58] X. Chen, P. Dai, D. L. Feng, T. Xiang, and F.-C. Zhang, *National Science Review* **1**, 371 (2014).
- [59] D.-H. Lee, *Chinese Physics B* **24**, 117405 (2015).
- [60] Z.-X. Li, F. Wang, H. Yao, and D.-H. Lee, *Science Bulletin* **61**, 925 (2016).
- [61] Y. Wang, A. Linscheid, T. Berlijn, and S. Johnston, *Phys. Rev. B* **93**, 134513 (2016).
- [62] S. Gerber, S.-L. Yang, D. Zhu, H. Soifer, J. A. Sobota, S. Rebec, J. J. Lee, T. Jia, B. Moritz, C. Jia, A. Gauthier, Y. Li, D. Leuenberger, Y. Zhang, L. Chaix, W. Li, H. Jang, J.-S. Lee, M. Yi, G. L. Dakovski, S. Song, J. M. Glownia, S. Nelson, K. W. Kim, Y.-D. Chuang, Z. Husain, R. G. Moore, T. P. Devereaux, W.-S. Lee, P. S. Kirchmann, and Z.-X. Shen, *Science* **357**, 71 (2017).
- [63] Y. Zhou and A. J. Millis, *Phys. Rev. B* **96**, 054516 (2017).
- [64] D. Huang and J. E. Hoffman, *Annual Review of Condensed Matter Physics* **8**, 311 (2017).
- [65] W. Zhao, M. Li, C.-Z. Chang, J. Jiang, L. Wu, C. Liu, J. S. Moodera, Y. Zhu, and M. H. W. Chan, *Science Advances* **4**, eaao2682 (2018).
- [66] D.-H. Lee, *Annual Review of Condensed Matter Physics* **9**, 261 (2018).
- [67] Q. Song, T. L. Yu, X. Lou, B. P. Xie, H. C. Xu, C. H. P. Wen, Q. Yao, S. Y. Zhang, X. T. Zhu, J. D. Guo, R. Peng, and D. L. Feng, *Nature Communications* **10**, 758 (2019).
- [68] S. Zhang, T. Wei, J. Guan, Q. Zhu, W. Qin, W. Wang, J. Zhang, E. W. Plummer, X. Zhu, Z. Zhang, and J. Guo, *Phys. Rev. Lett.* **122**, 066802 (2019).
- [69] Z.-X. Li, T. P. Devereaux, and D.-H. Lee, *Phys. Rev. B* **100**, 241101 (2019).
- [70] R. Peng, K. Zou, M. G. Han, S. D. Albright, H. Hong, C. Lau, H. C. Xu, Y. Zhu, F. J. Walker, and C. H. Ahn, *Science Advances* **6**, eaay4517 (2020).
- [71] S. A. Kivelson, D. S. Rokhsar, and J. P. Sethna, *Phys. Rev. B* **35**, 8865 (1987).
- [72] Z. Han, S. A. Kivelson, and H. Yao, *Phys. Rev. Lett.* **125**, 167001 (2020).
- [73] K. S. Huang, Z. Han, S. A. Kivelson, and H. Yao, *npj Quantum Materials* **7**, 17 (2022).
- [74] X. Cai, Z.-X. Li, and H. Yao, *Phys. Rev. Lett.* **127**, 247203 (2021).
- [75] S. R. White, *Phys. Rev. Lett.* **69**, 2863 (1992).
- [76] E. Jeckelmann and S. R. White, *Phys. Rev. B* **57**, 6376 (1998).
- [77] C. Hubig, I. P. McCulloch, U. Schollwöck, and F. A. Wolf, *Phys. Rev. B* **91**, 155115 (2015).
- [78] X. Cai, Z.-X. Li, and H. Yao, To appear soon.
- [79] See Supplemental Material for numerical details of the DMRG calculation (Sec. I), further data of the SC states (Sec. II), the evolution of pairing symmetry from *s*-wave to *d*-wave state (Sec. III), finite bond dimension extrapolations of DMRG (Sec. IV), as well as some results for the Holstein-Hubbard model on square lattice (Sec. V).
- [80] S. Raghu, S. A. Kivelson, and D. J. Scalapino, *Phys. Rev. B* **81**, 224505 (2010).
- [81] Q.-G. Yang, D. Wang, and Q.-H. Wang, *arXiv:2208.07036* (2022).
- [82] J. F. Dodaro, H.-C. Jiang, and S. A. Kivelson, *Phys. Rev. B* **95**, 155116 (2017).
- [83] C.-M. Chung, M. Qin, S. Zhang, U. Schollwöck, and S. R. White, *Phys. Rev. B* **102**, 041106 (2020).
- [84] G. Ehlers, S. R. White, and R. M. Noack, *Phys. Rev. B* **95**, 125125 (2017).
- [85] Y. Wang, Z. Chen, T. Shi, B. Moritz, Z.-X. Shen, and T. P. Devereaux, *Phys. Rev. Lett.* **127**, 197003 (2021).

SUPPLEMENTAL MATERIALS

A. Numerical details of DMRG calculation

Following the pseudo-site scheme in Ref. [76], we cut off the dimension of the local Hilbert space of the SSH phonon on each link to 2^M and then decompose the 2^M dimensional Hilbert space to M pseudo-sites of hard-core bosons. Fig. S1 shows the lattice geometry of the SSH model with two phonon pseudo-sites per link (the yellow circles), and the numbers around the (pseudo-)sites demonstrate how we map a 2D cylinder into a 1D matrix product state (MPS). Only the pseudo-sites with labels smaller than 21 are marked for clarity.

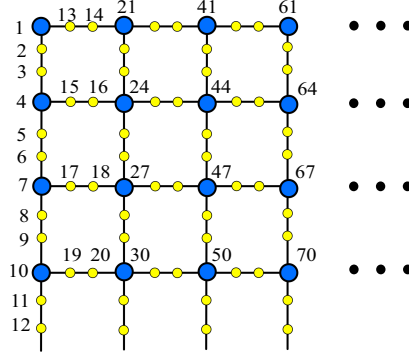


FIG. S1. The lattice geometry of 4-leg cylinder with $M = 2$ pseudo-sites on every bond of the square lattice. The blue circles represent fermion sites, while the yellow circles represent the pseudo-sites. The mapping of the cylinder to 1D MPS is arranged according to the labels of the sites.

Because all of the electron sites are surrounded by phonon pseudo-sites that do not involve the total electron number N or spin momentum S_z of electrons, the quantum numbers of the MPS' auxiliary bond cannot ascent automatically, even with the two-site update algorithm. To circumvent this issue of the EPC system, we implement the subspace expansion method [77] in the two-site update. By combining these two methods, we are able to obtain more accurate results at finite bond dimension D . In our code, we also parallel the contraction of the tensor to access higher bond dimension D and more reliable extrapolation of physical quantities as $D \rightarrow \infty$, or equivalently truncation error $\epsilon \rightarrow 0$.

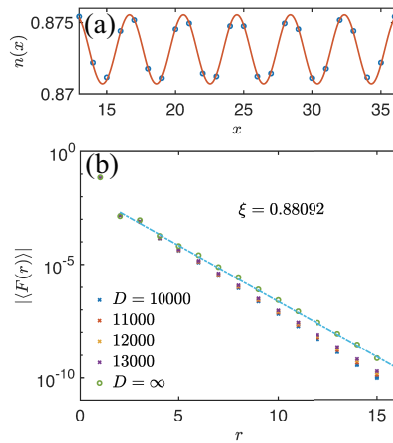


FIG. S2. (a) The charge density profile and (b) spin-spin correlation function of s -wave SC state on $L_x = 48$ cylinder with model parameter $U = 0$ and $\lambda = 0.3$.

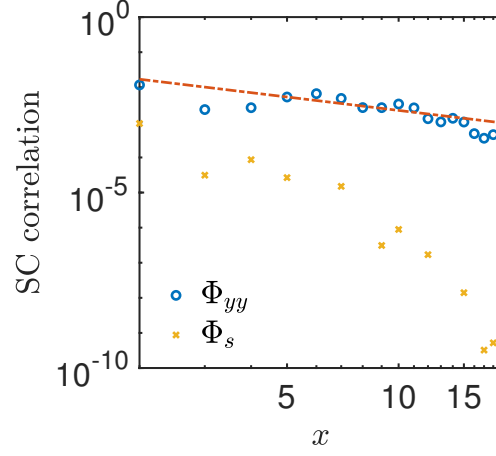


FIG. S3. SC correlation $\Phi_{yy}(x)$ and $\Phi_s(x)$ of $L_x = 40$ cylinder in d -wave state. The red dashed line is fitting of the exponent $K_{sc} = 1.27$.

B. Supplemental data for the s -wave state and the d -wave state

In this part, we show more results of observation as a complement to the main text. Figure S2 show the charge density profile and spin-spin correlation function of the s -wave state with model parameters $\lambda = 0.3$ and $U = 0$. Like the d -wave SC state, the period of the charge density distribution is 4 lattice constants. The spin correlation function decays exponentially with correlation length $\xi_s = 0.87$. Such a short correlation length indicates a spin gap in the s -wave SC ground state, consistent with the Luther-Emery liquid discussed in the main text.

In Fig. S3, we show the SC correlations Φ_{yy} and Φ_s in the $L_x = 40$ cylinder for the d -wave state. The model parameters are chosen as $\lambda = 0.3$ and $U = 8$ as in the main text. The d -wave SC correlation Φ_{yy} decays according to a power law with the exponent $K_{sc} \approx 1.2$. The exponent is slightly larger than that in the main text since the calculation does not completely converge with respect to the bond dimensions. We also discover an exponentially decaying s -wave SC correlation Φ_s , which is attributed to the suppression effect caused by the large on-site Coulomb repulsion U .

C. Evolution of pairing symmetry from s -wave to d -wave SC state

The Hubbard repulsion U , as mentioned in the main text, can significantly suppress the s -wave SC component while leaving the d -wave SC almost unchanged. Thus, a sufficiently large U can drive the system from s -wave SC state to d -wave SC state. To depict the evolution of the pairing symmetry as U increases, we calculate the SC correlations under different U in the s -wave SC phase and the d -wave phase with fixed EPC constant $\lambda = 0.3$. The results are shown in Fig. S4. For $U \leq 3$, the amplitudes of the s -wave SC correlation $\Phi_s(r)$ are stronger than those of the d -wave SC correlation $\Phi_{yy}(r)$, and both of them decay in the power law. The difference between the amplitudes of the s -wave and d -wave SC are decreasing as U approaches to 3. For large $U \geq 6$, the s -wave SC correlation decays much faster than d -wave SC correlation because of the suppression from the Coulomb repulsion. The evolution of the pairing symmetry supports the mechanism of the d -wave SC state discussed in the main text.

D. Finite bond dimension extrapolations

In this work, we used the second order polynomial function $O(\epsilon) = A\epsilon^2 + B\epsilon + C$ to extract the physical quantities $O(\epsilon \rightarrow 0)$, or equivalently $O(D \rightarrow \infty)$, where ϵ is the truncation error in the middle of the system for a given bond dimension D . In Fig. S5, we show two examples of the finite truncation error extrapolations of the charge density profile and SC correlation functions in the d -wave phase.

In Fig. S5(a), we calculate the electron density $n(x)$ with D varied from 9000 to 17000 and extrapolate $n(x, D = \infty)$ for each x using the second order polynomial function. The CDW amplitude $A_{CDW}(L_x)$ is extracted from $n(x, D = \infty)$

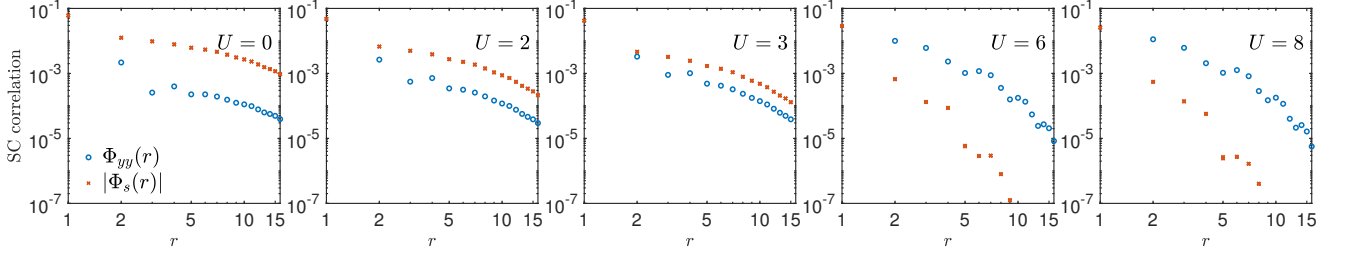


FIG. S4. The competitions between the s -wave pairing and the d -wave pairing when Hubbard repulsion U increases from 0 to 8 with fixed $\lambda = 0.3$. The data are obtained with finite bond dimensions $D = 8000 \sim 10000$. When U increases, the s -wave SC correlation is significantly suppressed, while the d -wave SC correlation remains nearly unchanged.

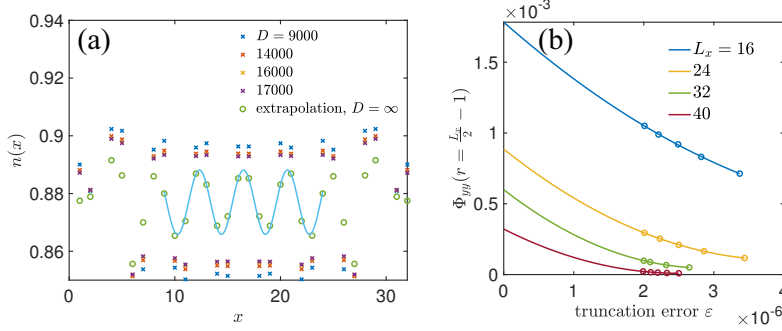


FIG. S5. Examples of finite truncation error extrapolation in d -wave SC phase with $U = 8, \lambda = 0.3$. (a) The charge density profile on $L_x = 32$ cylinder, where cross markers represent the data at finite bond dimensions, and circles represent the data after extrapolation. The CDW amplitude A_{CDW} is extracted from the blue curve in the central part of the cylinder by Eq. S1. (b) The extrapolation of SC correlation functions $\Phi_{yy}(r = L_x/2 - 1)$ on systems with different size.

in the middle of the cylinders by fitting the function

$$n(x) = A_{CDW} \cos(Q \cdot x + \theta) + n_0, \quad (S1)$$

where Q is the CDW ordering vector, $n_0 = 1 - \delta$ average charge density, θ is the non-universal phase factor. The result of L_x dependence of CDW amplitude $A_{CDW}(L_x)$ is shown in Fig. 2(c) in the main text. The extrapolation of SC correlation function $\Phi_{yy}(r = L_x/2 - 1)$ on systems with different $L_x = 16 \sim 40$ is directly shown in Fig. S5(b). For the largest $L_x = 40$ system, a much larger bond dimension is required to obtain reliable extrapolation. Limited by the computational resource, the accuracy of the Φ_{yy} on $L_x = 40$ cylinder is not as good as the one on the shorter cylinders. Consequently, the SC correlation $\Phi_{yy}(L_x/2 - 1)$ with $L_x = 40$ deviates from the power law decay slightly, as shown in Fig. 3(c) in the main text.

E. The Holstein-Hubbard model on square lattice

The Holstein-Hubbard model is defined as

$$H = -t \sum_{\langle i,j \rangle, \sigma} \left(c_{i,\sigma}^\dagger c_{j,\sigma} + \text{H.c.} \right) + \frac{U}{2} \sum_i n_i^2 + \alpha \sum_i n_i \hat{X}_i + \sum_i \left[\frac{\hat{P}_i^2}{2m} + \frac{k \hat{X}_i^2}{2} \right], \quad (S2)$$

where the phonon lives on site and couples with on-site electron density n_i . In the anti-adiabatic limit, one can integrate the optical phonon and get

$$H_{AA} = -t \sum_{\langle i,j \rangle, \sigma} \left(c_{i,\sigma}^\dagger c_{j,\sigma} + \text{H.c.} \right) + \frac{U_{eff}}{2} \sum_i n_i^2 \quad (S3)$$

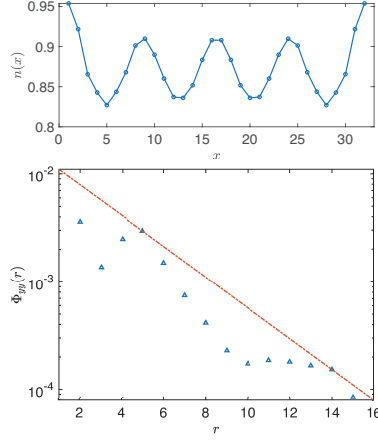


FIG. S6. Charge density profile and SC correlation for the Holstein-Hubbard model on $L_x = 32$ cylinder with model parameters $U = 8$ and $\lambda = 0.2$. The data are obtained at finite keep state $D = 14000$.

with effective interaction $U_{eff} = U - \alpha^2/k$. Here, the instantaneous phonons only renormalize the Hubbard repulsion U to a weaker value.

We calculate the Holstein-Hubbard model with $\omega = 5$, $\lambda = 0.2$, and $U = 8$ on four-leg cylinders. At doping level $\delta = 1/8$, the ground state is a filled-stripped state, the same as the one of the pure Hubbard model. The charge density profile and the SC correlation functions of the ground state are shown in Fig. S6. The wavelength of CDW order is 8 lattice constants and the SC correlation decay exponentially fast correlation length $\xi_{SC} = 3.04$.